Journal of Power Sources 217 (2012) 108–113

Contents lists available at SciVerse ScienceDirect

Journal of Power Sources

journal homepage: www.elsevier.com/locate/jpowsour

Short communication

Influence of the binder types on the electrochemical characteristics of tin nanoparticle negative electrode for lithium secondary batteries

Guichang Liu [a,*], Xiaoxiao Shen [a], Koichi Ui [b], Lida Wang [a], Naoaki Kumagai [b]

[a] Department of Material Science and Chemical Engineering, School of Chemical Engineering, Dalian University of Technology, No. 2, Linggong Road, Dalian 116024, China
[b] Frontier Materials and Function Engineering, Graduate School of Engineering, Iwate University, Morioka 020 8551, Japan

HIGHLIGHTS

- The cycle performances of the tin nanoparticle electrodes are shown in the figure.
- The use of the CMC binder improved the initial discharge capacity.
- The use of the CMC binder improved the cyclic retention.
- The addition of acetylene black into the electrode further improved the cycle performance.

GRAPHICAL ABSTRACT

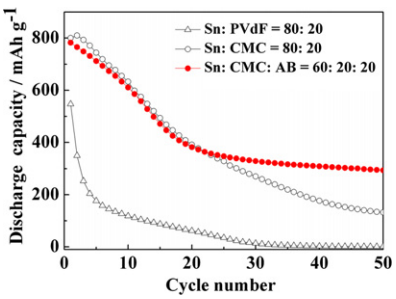

ARTICLE INFO

Article history:
Received 5 January 2012
Received in revised form
29 May 2012
Accepted 30 May 2012
Available online 9 June 2012

Keywords:
Tin
Nanomaterial
Negative electrode
Lithium secondary battery
Binder
Carboxymethyl cellulose

ABSTRACT

The influence of the binder types on the electrochemical characteristics of the tin nanoparticle negative electrode for lithium secondary batteries has been investigated using cyclic voltammetry, charge–discharge test, electrochemical impedance spectroscopy, scanning electron microscope, and transmission electron microscope. The results show that the initial capacity and the cyclic retention of the tin electrode using carboxymethyl cellulose as a binder are better than those of using polyvinylidene fluoride as a binder. Moreover, the cycle performance is further enhanced by the addition of acetylene black into the electrodes using the carboxymethyl cellulose binder. The good capacity retention in the subsequent cycles may be attributed to the formed branch-like structure on the surface of the tin nanoparticles during cycling.

1. Introduction

The fast developing technologies for portable electronic devices and electric vehicles call for lithium-ion batteries with high energy density. Tin, as a candidate anode material of lithium-ion batteries, has received much attention because of its much higher specific capacity (994 mAh g^{-1}) than that of commercially used graphite (372 mAh g^{-1}). However, tin anodes usually perform poor cyclic retentions due to the huge volume changes during charge/discharge process [1,2]. It has been proved that the bulk tin material could easily crack during cycling, which would directly increase the resistance of the electrode. Many efforts have been made to improve the capacitance and the cycle ability of the tin-based material. Up to now, there are mainly two strategies: one is to make tin-based alloys or composites with other materials such as Ni, Co, and carbon, which act as matrix for tin in the charge/discharge process [3–9]; the other is to turn to nanosized materials [1,10,11] due to the

* Corresponding author. Tel./fax: +86 411 84986047.
E-mail addresses: gchliu@dlut.edu.cn (G. Liu), xiaoxiao.shen421@gmail.com (X. Shen).

0378-7753/$ – see front matter © 2012 Elsevier B.V. All rights reserved.
http://dx.doi.org/10.1016/j.jpowsour.2012.05.116

fact that reducing the particle size of the active material can alleviate this problem to some extent [12]. Besides, some studies were also based on the combination of the two strategies [7,13–16]. In addition to the active material, other parts such as a binder and a conductive agent also have significant influences on the electrochemical performance. The binder used in the electrode has a significant impact on the properties of active material. There have emerged new water-soluble binders, such as polyacrylate [17] and carboxymethyl cellulose (CMC) [18–24]. Among these binders, CMC has been successfully used for the carbon-coated SnO_2 [18] and the Si [25] anodes due to their accommodation of volume change during cycling [24] and environmental-friendly features. However, the effect of CMC on the electrochemical characteristics of tin nanoparticle is still not clear.

In this study, we aim to investigate the electrochemical characteristics of the tin nanoparticle by comparing the CMC binder with the conventional polyvinylidene fluoride (PVdF) binder. Meanwhile, the effect of the addition of conductive agent acetylene black (AB) on the electrochemical properties of the tin nanoparticle electrode is also discussed.

2. Experimental

2.1. Preparation of tin nanoparticle anode

A tin nanoparticle (<100 nm, 99.7+%, Aldrich) was mixed with PVdF (Kureha, KF#9130) or CMC (average Mw: ~330, 000, Daicel Co. Ltd.) as binders, and then dissolved in N-Methy1-2-pyrrolidone or distilled water, respectively. The weight ratios of tin nanoparticle and the binders are both 80:20 for the electrodes without any conductive agent. For the electrodes added AB, the tin nanoparticle, the CMC binder, and AB were mixed as a weight ratio of 60:20:20. After stirring for 24 h, the slurries were uniformly coated onto nickel meshes with an effective electrode area of 2 cm^2. After drying at 80 °C for 1 h to remove most of the solvent, the electrodes were dried at 180 °C under reduced pressure for 3 h.

2.2. Cells assembling and electrochemical tests

Three-electrode experimental cells were assembled with the as-prepared electrodes as working electrodes, lithium foils as both counter and reference electrodes in an Ar-filled glove box (Miwa Mtg Co., Ltd., DBO-1NKP-1V-2). The electrolyte was 1 mol dm^{-3}(M) $LiClO_4$ dissolved in the 1:1 (vol.) mixture of ethylene carbonate (EC) and diethyl carbonate (DEC)(Mitsubishi Chemical Co.; water content under 20 ppm). All cells were galvanostatically charged and discharged in a battery test system (Hokuto Denko, HJR-1010mSM8) at a current density of 99.4 mA g^{-1} ($1C = 994$ mA g^{-1}) under a cut-off potential range of 0.1–2.0 V. All the potentials in this study are with respect to Li/Li^+ electrode. Cyclic voltammetry (CV) was carried out by an electrochemical system (Hokuto Denko, HZ-5000) at a scan rate of 0.1 mV s^{-1} under the same potential range with charge/discharge test. Current density and specific capacity were calculated based on the mass of tin nanoparticles in the electrode. The electrochemical impedance spectroscopy (EIS) of the tin nanoparticle electrodes was conducted by applying a sine wave with an amplitude of 10 mV in the frequency range from 100 kHz to 100 mHz. All electrochemical measurements were carried out at 25 °C.

2.3. SEM and TEM observations

The surface morphology characterizations of the electrodes were carried out by using scanning electron microscope (SEM; 15 kV, JSM 7001) and transmission electron microscope (TEM; 200 kV, Hitachi, H-800).

3. Results and discussion

The cyclic voltammogram in Fig. 1(a) and (b) show that the electrode using CMC displays a much higher current density than that of using PVdF in the initial cycle, and the current density maintains stable in the following two cycles, indicating better cyclic retention of the electrode using CMC. In the case of CMC, the peak around 1.0 V in the cathodic process may involve three parts: the reduction of the electrolyte to form an SEI (solid electrolyte interface) film, the reduction of tin oxide that formed when the electrodes were exposed in the air during the preparation of the electrodes [26], and some reductive reactions of CMC. El Ouatani et al. [22] found that the chemical reactivity of CMC towards the electrolyte takes part in the formation of the surface film, and contributes to the good properties of CMC as binder, and the reaction of CMC towards the electrolyte do not disappear upon electrochemical cycling. So in Fig. 1(b) and (c), the reversible peaks in the cathodic range around 1.0 V and the anodic hump from 1.0 to

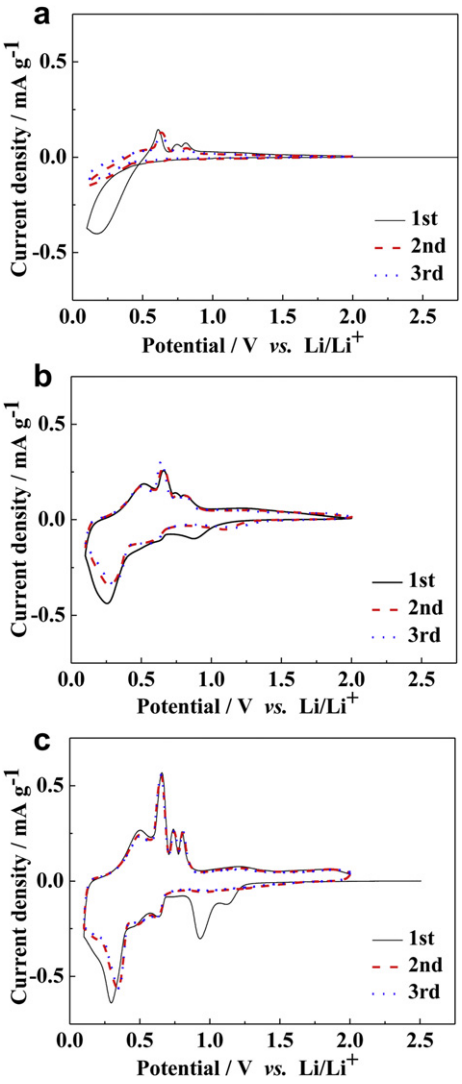

Fig. 1. Cyclic voltammograms of the tin nanoparticle electrodes using (a) 20 wt.% PVdF as a binder, (b) 20 wt.% CMC as a binder, and (c) the CMC binder (20 wt.%) with 20 wt.% AB as a conductive additive. Potential range: 0.1–2.0 V *vs.* Li/Li^+, scan rate: 0.1 mV s^{-1}.

1.5 V may derive from the reactions of $-CH_2COOH$ and $-OH$ groups of CMC. The peaks shown in the range of 0.5–0.1 V in the charging process and the three peaks in the discharging process are ascribed to the lithiation and delithiation reactions, respectively. With the addition of AB, the current densities of the peaks were greatly enhanced, and without being a big hump in the relevant range, the peaks become more individual to each other. The irreversible peaks during the first cathodic process at 1.1 V and 0.9 V are the reduction of electrolyte and tin oxide, respectively [27]. Except for the irreversible reaction peaks, the curves were almost overlapped in the three cycles, indicating that the addition of conductive agent AB can improve the cyclic retention of the electrodes.

Fig. 2 shows the charge–discharge curves of the tin nanoparticle electrodes using PVdF and CMC binder for the 1st, 2nd, 5th, 10th and 50th cycles. From Fig. 2(a), the discharge capacity of the electrode using PVdF fades quickly from the initial 548 mAh g^{-1} to 118 mAh g^{-1} after 10 cycles, further indicating PVdF is not an effective binder for tin nanoparticle electrode. Moreover, there is a sudden backtracking after the voltage reached 0.4 V in the initial charging curve, consequently resulting in a hump at about 0.7 V. In the following cycles, the hump disappeared, which means that this process is irreversible. In contrast, the electrode using CMC binder (Fig. 2(b)) displays a higher capacity and better capacity retention over the ten cycles. In addition, the voltage profile for the first charging process is stable. The electrode shows an initial charge–discharge efficiency of 65.4%, which is slightly lower than that of using PVdF (67.2%). The irreversible capacity loss in the first cycle is mainly due to the SEI formation on the surface of the electrodes and the reduction of the tin oxide formed during the preparation process of the electrodes [3,4]. Fig. 2(c) shows that although the electrode added AB display a slightly lower initial capacity as compared to that of electrode without AB, the addition of AB increases the charge–discharge efficiency of the first cycle to 75.8%, which could be due to less tin oxide was formed on the surface of tin nanoparticle, owing to the reduction property of carbon.

The cycle performances of the electrodes in Fig. 3 reveal that the discharge capacities for all the electrodes decreased quickly in the first 20 cycles. Particularly, the discharge capacity of the electrode using PVdF binder declines rapidly during the initial 5 cycles, and almost no capacity has retained after 30 cycles. The electrode using CMC binder without conductive agent displays a better cycle performance compared to that of using PVdF. which may be attributed to the effective binding between CMC and the active material [28]. After 20 cycles, the capacity loss for the electrodes with AB changes slower than that of without AB. After 50 cycles, the discharge capacities for the electrodes using CMC without AB and with 20 wt.% AB are 132 and 293 mAh g^{-1}, respectively. This result suggests that the addition of certain amount of AB is useful to improve the capacity retention for the tin nanoparticle anode. In Fig. 3(b), the efficiency of the electrode using PVdF increases gradually during the initial cycles, especially in the first 5 cycles,

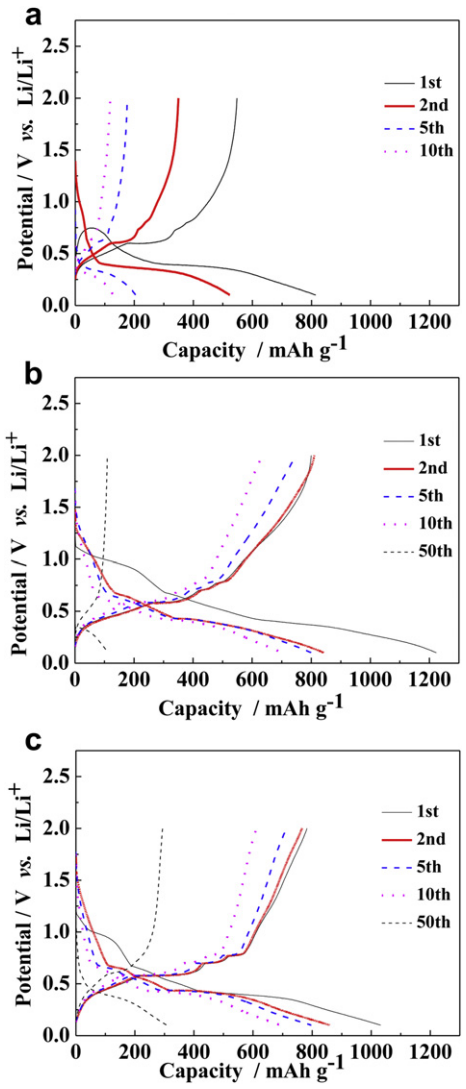

Fig. 2. Charge–discharge curves of the tin nanoparticle electrodes using (a) 20 wt.% PVdF as a binder, (b) 20 wt.% CMC as a binder, and (c) the CMC binder (20 wt.%) with 20 wt.% AB as a conductive additive. Potential range: 0.1–2.0 V *vs.* Li/Li^+, current density: 99.4 mA g^{-1} (0.1 *C*).

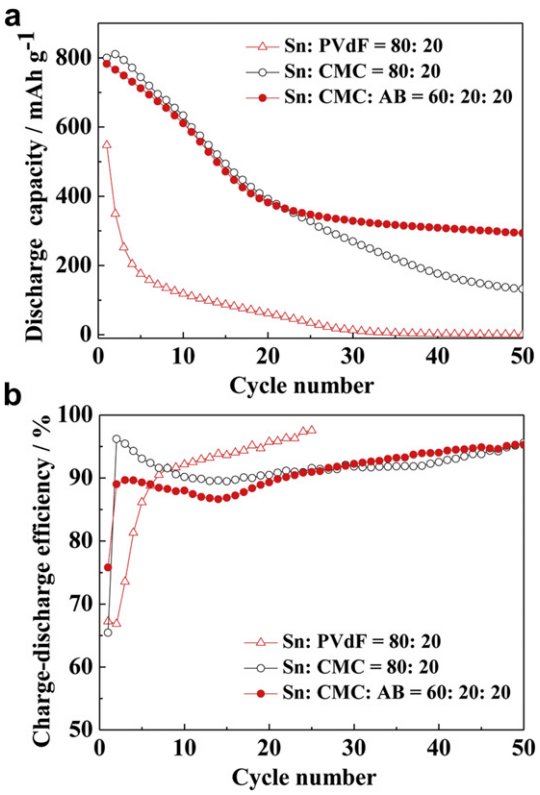

Fig. 3. Cycle performance of the tin nanoparticle electrodes: (a) cycle number *vs.* discharge capacity of all the three electrodes, (b) cycle number *vs.* charge–discharge efficiency. Potential range: 0.1–2.0 V *vs.* Li/Li^+, current density: 99.4 mA g^{-1} (0.1 *C*).

which is different from that of using CMC binder. It suggests that an effective SEI film was not formed in the first cathodic process, which also conduces to the fast capacity fading during the following cycles. The efficiency keeps over 90% after 10 cycles, which implies that although charge capacity drops fast, the irreversible capacity loss in each cycle is not high. The poor cyclic retention of the electrode using PVDF is mainly blame for the incapability in the lithiation process. The efficiency data of the electrode using PVDF binder presented here is only for the initial 25 cycles, because the data after 25 cycles was of little point due to the low capacity. The charge–discharge efficiency for the electrodes using CMC binder is kept at more than 85% after the first cycle. After 25 cycles, the electrode with 20 wt.% AB kept a higher efficiency, suggesting that a better reversible reaction during cycling were maintained.

SEM images in Fig. 4 show that in the case of PVdF, the tin nanoparticles display no apparent change in particle size after the initial charge and discharge processes. It suggests that the active material didn't sufficiently react with lithium ion, which is in agreement with the results of electrochemical tests. In contrast, the particles bond with CMC show huge volume expansion after the first charging process and obvious shrinkage after the discharge process. The electrodes using CMC binder with 20 wt.% AB show a larger surface area before charge–discharge process, and after the discharge process a structure with much open space was formed, suggesting that CMC binder and AB together supply a good accommodation for the huge volume change of tin during cycling.

Fig. 5 shows the TEM images of the tin nanoparticle electrodes using CMC binder. Fig. 5(a) and (e) show that the tin nanoparticles were bound together by the binder. The tin nanoparticles expanded and shrinked after charge and discharge test, respectively, which is in line with the SEM images in Fig. 4. Besides, the electrode using CMC 20 wt.% and AB 20 wt.% shows a branch-like structure on the edge of the tin nanoparticle (Fig. 5(h)), which is not shown in Fig. 5(d). We explain it as follows. With the proceeding of cycling, the edge of the particles becomes vague, and a layer of branch-like structure is formed on the surface of the particles, which enhances the dimensional stability by supplying a buffering effect against the volume expansion of the particle during cycling, and this may contribute to the stable electrochemical performance in the following cycles. This structure may display a similar function with the multilayer structure in ref. [29].

To better understand the reason for the better cycle performance when AB was added into the electrodes which use the CMC binder, EIS measurements were conducted after discharging the electrodes up to 2.0 V, a namely 100% delithiation state. The EIS plots for both AB-free and AB-added electrodes after 1st, 10th, 25th and 50th cycles are presented in Fig. 6(a) and (b), respectively. The inset figures are the zoom part at the high-frequency range. A typical Nyquist plot for a lithium secondary battery should comprises two semicircles in high-frequency and medium-frequency ranges and a line inclined at an approximate 45° angle to the real axis in low frequency [30]. The two semicircles are ascribed to SEI film and the interfacial charge-transfer and the linear part to $Li+$ diffusion process within the electrode. In Fig. 6(a), all the Nyquist plots show a depressed semicircle in the high-frequency region and an arc in the medium and low frequency range. The semicircle may correspond to the SEI film, and the arc should refers to the charge-transfer process, which is too low to be measured because the impedance of this process is too high and the

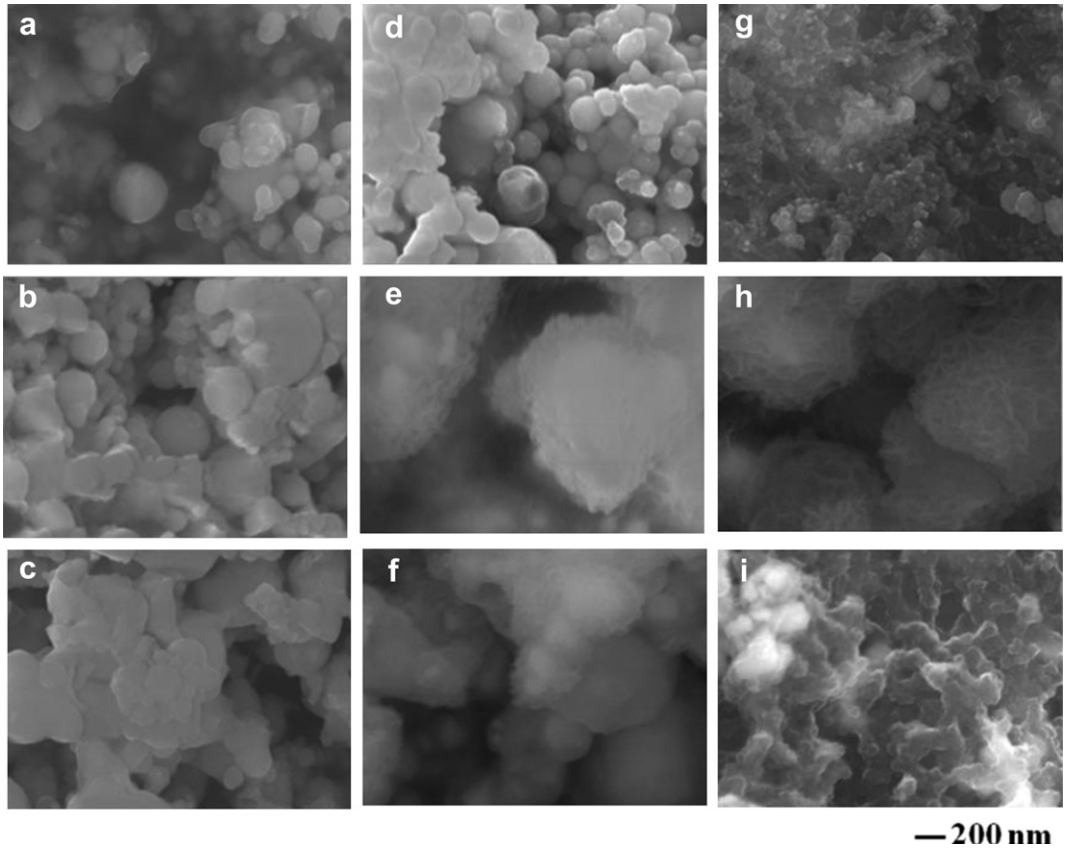

Fig. 4. SEM images of the tin nanoparticle electrodes as-prepared (upper), after 1st charging (middle), and after 1st discharging (bottom). The tin nanoparticle electrodes prepared by using the PVdF binder (a, b, c), using the CMC binder (d, e, f) and using CMC 20 wt.% with AB 20 wt.% (g, h, i).

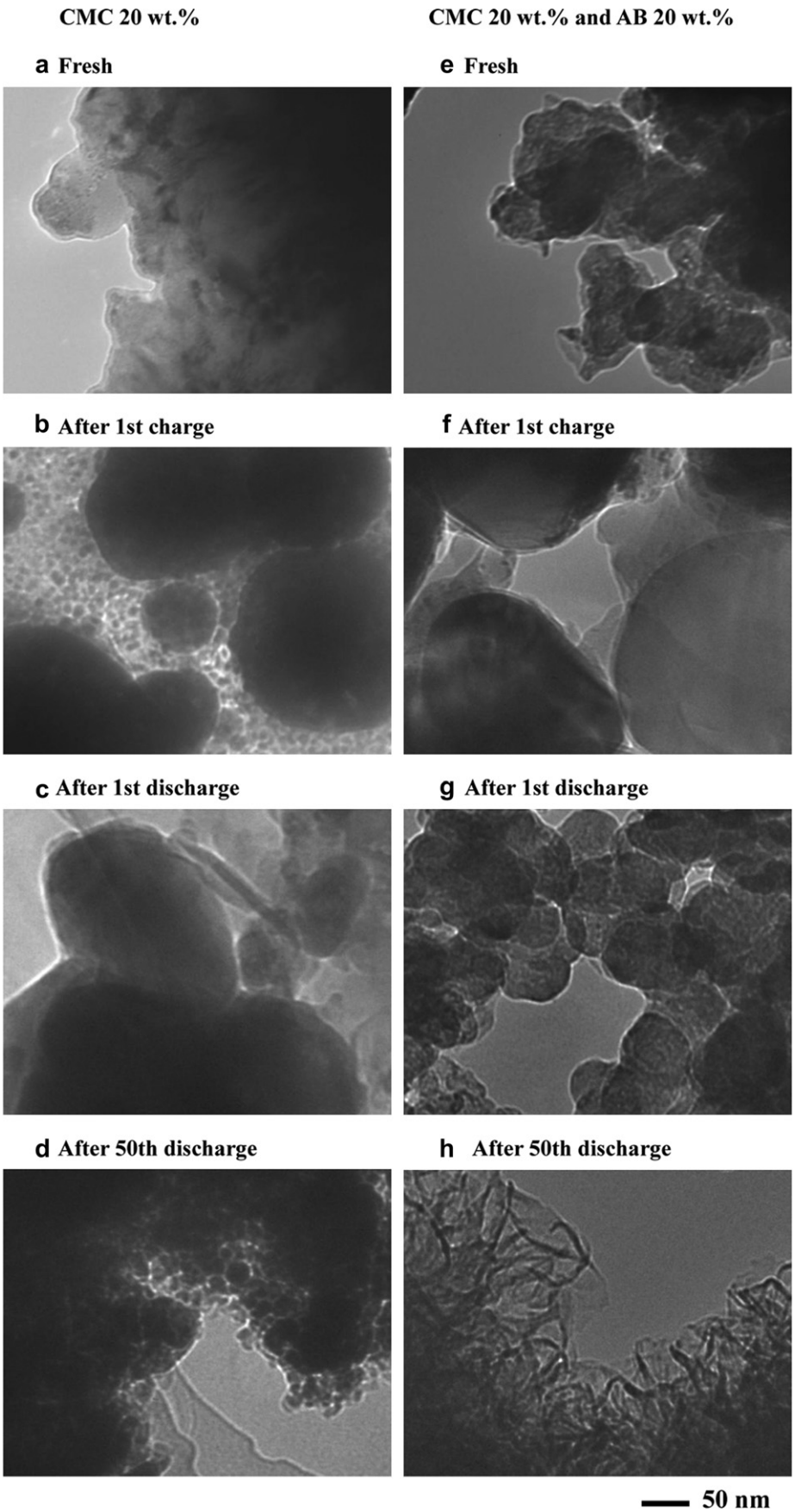

Fig. 5. TEM images of the tin nanoparticle electrodes as-prepared (upper), after 1st charging (second layer), after 1st discharging (third layer), and after 50th discharging (bottom). The tin nanoparticle electrodes prepared by using the CMC binder (a, b, c, d), and using CMC 20 wt.% with AB 20 wt.% (e, f, g, h).

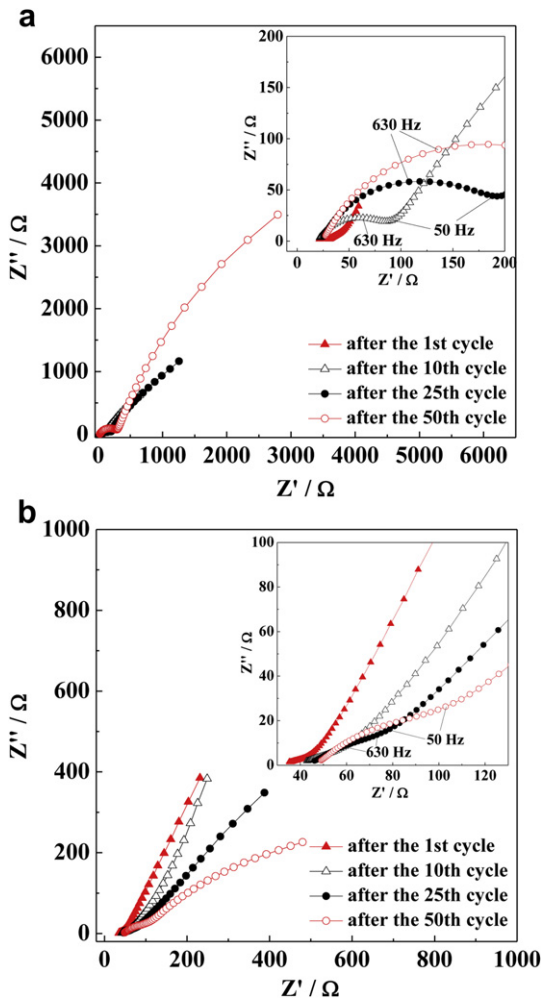

Fig. 6. Nyquist plots of the tin nanoparticle electrode with CMC 20 wt.% (a), and the tin nanoparticle electrode with CMC 20 wt.% and AB 20 wt.% (b) after different numbers of cycles.

semicircle cannot be formed in this fully delithiated state [31]. The diameter of the semicircle increased with the increasing of cycling number, indicating the resistance of the SEI film increases during cycling, which may be attributed to the change in the electrode surface condition (surface area and chemical composition) caused by the voltage change of the tin nanoparticles and reactions between CMC and the electrolyte. This change in the impedance of SEI film also explains the fading of cycle performance to some extent. In Fig. 6(b), the Nyquist plots of the electrode added AB displays no obvious semicircle in the high-frequency range for the 1st and 10th cycle, which means the impedance of the SEI film is relatively low comparing to the electrode bulk. However, when the EIS test was further performed, the EIS plots tested after 25th and 50th cycle show an arc in the high-frequency range, which should be the impedance of the SEI film. The EIS results show that the impedance of the SEI film decreases when AB was added into the electrode, and also explain that the surface state of the electrodes changes during cycling.

4. Conclusions

In this study, we reported the electrochemical performance of tin nanoparticle anodes using traditional binder PVdF and new water-soluble binder CMC. The binder type plays an important role in the enhancement of electrochemical performance for tin nanoparticle anodes, and the addition of AB further improve the cycle performance of the tin nanoparticle electrodes using CMC. However, the electrodes using CMC binder still undergo rapid capacity fading in the first 20 cycles. Further work such as optimize the preparing condition of the tin nanoparticle electrode is still needed.

References

[1] T. Zhang, L.J. Fu, J. Gao, Y.P. Wu, R. Holze, H.Q. Wu, J. Power Sources. 174 (2007) 770.
[2] S.F. Yang, P.Y. Zavalij, M.S. Whittingham, Electrochem. Commun. 5 (2003) 587.
[3] H. Li, Z.X. Wang, L.Q. Chen, X.J. Huang, Adv. Mater. 21 (2009) 4593.
[4] A. Aboulaich, M. Mouyane, F. Robert, P.E. Lippens, J. Olivier-Fourcade, P. Willmann, J.C. Jumas, J. Power Sources. 174 (2007) 1224.
[5] M. Mouyane, J.M. Ruiz, M. Artus, S. Cassaignon, J.P. Jolivet, G. Caillon, C. Jordy, K. Driesen, J. Scoyer, L. Stievano, J. Olivier-Fourcade, J.C. Jumas, J. Power Sources. 196 (2011) 6863.
[6] L. Huang, H.B. Wei, F.S. Ke, X.Y. Fan, J.T. Li, S.G. Sun, Electrochim. Acta. 54 (2009) 2693.
[7] G. Derrien, J. Hassoun, S. Panero, B. Scrosati, Adv. Mater. 19 (2007) 2336.
[8] J. Hassoun, G. Mulas, S. Panero, B. Scrosati, Electrochem. Commun. 9 (2007) 2075.
[9] J. Xie, G.S. Cao, X.B. Zhao, Y.D. Zhong, M.J. Zhao, J. Electrochem. Soc. 151 (2004) A1905.
[10] K.T. Lee, J. Cho, Nano Today. 6 (2011) 28.
[11] L. Bazin, S. Mitra, P.L. Taberna, P. Poizot, M. Gressier, M.J. Menu, A. Barnabe, P. Simon, J.M. Tarascon, J. Power Sources. 188 (2009) 578.
[12] K. Ui, S. Kikuchi, Y. Kadoma, N. Kumagai, S. Ito, J. Power Sources. 189 (2009) 224.
[13] S. Liu, Q. Li, Y.X. Chen, F.J. Zhang, J. Alloys and Comp. 478 (2009) 694.
[14] Y.H. Yu, Q. Yang, D.H. Teng, X.P. Yang, S. Ryu, Electrochem. Commun. 12 (2010) 1187.
[15] L. Balan, R. Schneider, J. Ghanbaja, P. Willmann, D. Billaud, Electrochim. Acta. 51 (2006) 3385.
[16] X.Y. Zhao, Z.H. Xia, D.G. Xia, Electrochim. Acta. 55 (2010) 6004.
[17] J. Li, D.B. Le, P.P. Ferguson, J.R. Dahn, Electrochim. Acta. 55 (2010) 2991.
[18] S.L. Chou, J.Z. Wang, C. Zhong, M.M. Rahman, H.K. Liu, S.X. Dou, Electrochim. Acta. 54 (2009) 7519.
[19] J.H. Lee, Y.M. Choi, U. Paik, J.G. Park, J. Electroceram. 17 (2006) 657.
[20] H. Buqa, M. Holzapfel, F. Krumeich, C. Veit, P. Novak, J. Power Sources. 161 (2006) 617.
[21] W. Zaidi, Y. Oumellal, J.P. Bonnet, J. Zhang, F. Cuevas, M. Latroche, J.L. Bobet, L. Aymard, J. Power Sources. 196 (2011) 2854.
[22] L. El Cualtania, R. Dedryvere, J.B. Ledeuil, C. Siret, P. Biensan, J. Desbrieres, D. Gonbeau, J. Power Sources. 189 (2009) 72.
[23] D. Munao, J.W.M. van Erven, M. Valvo, E. Garcia-Tamayo, E.M. Kelder, J. Power Sources. 196 (2011) 6695.
[24] F.M. Courtel, S. Niketic, D. Duguay, Y. Abu-Lebdeh, I.J. Davidson, J. Power Sources. 196 (2011) 2128.
[25] N. Ding, J. Xu, Y.X. Yao, G. Wegner, I. Lieberwirth, C.H. Chen, J. Power Sources. 192 (2009) 644.
[26] X.L. Wang, M. Feygenson, M.C. Aronson, W.Q. Han, J. Phys. Chem. C. 114 (2010) 14697.
[27] R. Demir-Cakan, Y.S. Hu, M. Antonietti, J. Maier, M.M. Titirici, Chem. Mater. 20 (2008) 1227.
[28] N.S. Hochgatterer, M.R. Schweiger, S. Koller, P.R. Raimann, T. Wohrle, C. Wurm, M. Winter, Electrochem. Solid-State Lett. 11 (2008) A76.
[29] R. Kim, D. Nam, H. Kwon, J. Power Sources. 195 (2010) 5067.
[30] S.S. Zhang, K. Xu, T.R. Jow, Electrochim. Acta. 49 (2004) 1057.
[31] S.S. Zhang, K. Xu, T.R. Jow, Electrochim. Acta. 51 (2006) 1636.